ELSEVIER

International Journal of Heat and Fluid Flow 23 (2002) 137–147

International Journal of HEAT AND FLUID FLOW

www.elsevier.com/locate/ijhff

Elevated freestream turbulence effects on heat transfer for a gas turbine vane

K.A. Thole [a,*], R.W. Radomsky [b], M.B. Kang [c], A. Kohli [c]

[a] *Mechanical Engineering Department, Virginia Polytechnic Institute and State University, Blacksburg, VA 24061, USA*
[b] *United Technologies Research Center, 411 Silver Spring Lane, East Hartford, CT 06108, USA*
[c] *Pratt and Whitney, 400 Main Street, East Hartford, CT 06108, USA*

Abstract

High freestream turbulence levels have been shown to greatly augment the heat transfer along a gas turbine airfoil, particularly for the first stage nozzle guide vane. For this study, augmentations in convective heat transfer have been measured for a first stage turbine vane in the stagnation region, along the mid-span, and along the platform resulting from an approach freestream turbulence level of 19.5%. In addition to quantifying surface heat transfer, boundary layer measurements have been made to better understand high freestream turbulence effects. Although there are a number of correlations that have been developed for scaling freestream turbulence augmentations to heat transfer, the results of this study indicate that these correlations are not successful in predicting heat transfer for various regions along a turbine vane.

1. Introduction

Accurate predictions of surface heat loads on an airfoil are made difficult by the complex flow structure surrounding the airfoil. Boundary layers developing on a vane or blade surface are subjected to a combination of variables including freestream turbulence, surface curvature, roughness, favorable and adverse pressure gradients, boundary layer transition, relaminarization and stagnation point flow. Numerous investigations have been performed in the past that have addressed the isolated effects of most of these variables on boundary layer development with the majority of the studies being performed on simple flat plate or cylinder-in-crossflow geometries. To incorporate all of the variables affecting boundary layer development on gas turbine airfoils, studies need to be performed on a representative airfoil geometry.

Turbulence measurements taken at the exit of a variety of gas turbine combustors have shown that the levels can range between 8% and 40% (Kuotmos and McGuirk, 1989; Goebel et al., 1993) with an indication that the integral length scale is dictated by the diameter of the dilution holes in the combustor (Barringer et al., 2001). Although the turbulent kinetic energy levels actually increase through the downstream airfoil passage due to the velocity gradients experienced by the flow (Radomsky and Thole, 2000a), the local turbulence levels, particularly along the suction side, decrease as the flow is accelerated. The effect that these high turbulence levels have on the airfoil is to significantly increase the heat transfer along the leading edge and pressure side surfaces as well as move the transition location forward on the suction side surface.

The objective of this paper is to present augmentations of convective heat transfer due to freestream turbulence for three distinct regions of a first stage nozzle guide vane. Those regions include the stagnation location, along the mid-span section of the turbine vane, and along the platform (endwall) of the turbine vane. The reason for choosing the stagnation and platform regions is because it is in these locations where airfoil durability is often an issue. Although no correlations are available for the platform region, previously presented correlations for the stagnation and mid-span of the vane will be evaluated for scaling heat transfer augmentations on a turbine vane.

* Corresponding author. Tel.: +1-540-231-7192; fax: +1-540-231-9100.
E-mail address: thole@vt.edu (K.A. Thole).

0142-727X/02/$ - see front matter
PII: S0142-727X(01)00145-X

Nomenclature

a	freestream strain rate, dU/dx
b	turbulence generator bar width
C	true chord of stator vane
C_f (C_{fo})	friction coefficient (low turbulence case), $2(u_\tau^2/U_{edge}^2)$
C_p	specific heat
d	effective diameter
h	convective heat transfer coefficient
L_a	length scale parameter, $\Lambda_x/\sqrt{v/a}$
L_ε	dissipation length scale, $1.5u_{rms}^2/\varepsilon$
k	turbulent kinetic energy, $0.5(u_{rms}^2+v_{rms}^2+w_{rms}^2)$
K	acceleration parameter, $v(dU_{edge}/ds)/U_{edge}$
Nu_a	modified Nusselt number, $h/k\sqrt{a/v}$
P	vane pitch
Pr	Prandtl number
Re	Reynolds number, sU/v
Re_{in}	Reynolds number, CU_{in}/v
s	surface distance along vane measured from stagnation
S	span of vane
$St(St_0)$	Stanton number (low turbulence case), $h/\rho C_p U$
St'	Stanton number based on urms, $h/\rho C_p u_{rms}$
TLR	turbulence parameter, $Tu(\theta/\Lambda_x)^{0.33}\times(Re_\theta/1000)^{0.25}$
TL_t^+	modified turbulence level (Eq. (1))
Tu	turbulence level $(0.5(u_{rms}^2+v_{rms}^2))^{0.5}/U_{edge}$
Tu_λ	modified turbulence level, $(\sqrt{L_a}u_{rms}/\sqrt{av})/(1+0.004L_a^2)^{5/12}$
u_τ	shear velocity, $\sqrt{\tau_w/\rho}$
u^+	velocity in inner coordinates, u/u_τ
U_{inlet} (U_∞)	incident upstream velocity
U_{edge}	local inviscid velocity
U, V, W	mean velocity in the X, Y, Z directions
X, Y, Z	global coordinates defined from stagnation location
y^+	velocity in inner coordinates, yu_τ/v

Greeks

δ, θ	boundary layer thickness and momentum thickness
ε	turbulent dissipation rate
Λ_x	integral length scale
Λ_x^+	integral length scale in inner coordinates, $\Lambda_x u_\tau/v$
ρ	density
τ_w	wall shear stress
v	viscosity

Subscripts

edge	local inviscid quantity
inlet	inlet
rms	root mean square

2. Previous studies

Previously presented correlations available for the vane mid-span section are based on flat plate studies with elevated turbulence levels. These flat plate studies date back to Kestin (1966). Three correlations have been repeatedly evaluated for scaling surface heat transfer with elevated freestream turbulence levels for a flat plate boundary layer. Those correlations include Hancock and Bradshaw's β parameter (Hancock and Bradshaw, 1983), the Ames and Moffat's TLR parameter (Ames and Moffat, 1990), and the Maciejewski and Moffat's St' correlation (Maciejewski and Moffat, 1992). In particular, the turbulence levels that were considered for the latter two studies were with the intention of scaling turbulence effects with levels being applicable to those found in a gas turbine, i.e., 20%. In a paper by Thole and Bogard (1995), these correlations were evaluated for scaling a number of different data bases indicating that the TLR parameter had the most success; however, as the turbulence levels approached 20% the St' model became more applicable and was successful in collapsing the data.

Barrett and Hollingsworth (1999) presented an alternative Stanton number correlation for high freestream turbulence effects. This correlation is a function of core flow parameters such as length scale and turbulence level as shown below.

$$TL_t^+ = \frac{0.128\sqrt{C_f/2}}{1.38+\frac{0.28}{Tu}\sqrt{C_f/2}\left[\left(1-e^{15/\Lambda_x^+}\right)+1.4e^{-1.7(15/\Lambda_x^+)}\left(15/\Lambda_x^+\right)^{2/3}\right]^{-1/2}}.$$

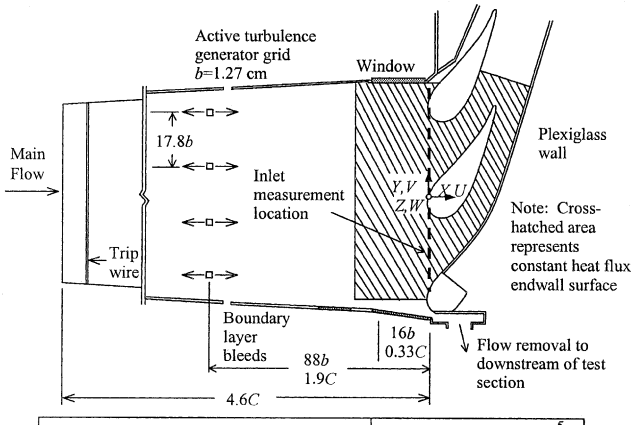

Scaling factor	9	Re_{in}	2.3×10^5
Scaled-up true chord	59.4 cm	U_{inlet}	5.85
Pitch/true chord	0.77	T_{inlet}	20°C
Span/true chord	0.93		

Fig. 1. Schematic of stator vane test section.

It is not relevant to consider the platform region of a turbine airfoil as a flat plate because of the predominantly three-dimensional flow field that is present. No known correlations (and relatively little data) depicting the augmentation due to high turbulence levels exists for this region. For the stagnation location of the vane, correlations previously presented by Dullenkopf and Mayle (1995), which account for the freestream strain rate, and modified turbulence level and length scale, will be evaluated. The stagnation location correlation was developed from both cylinder and airfoil data.

The remainder of this paper discusses the experimental facility used to acquire the heat transfer and flow field data, for each of the three regions of the airfoil, and a comparison of the available correlations.

3. Experimental design

The details of the recirculating wind tunnel and design of the stator vane test section used in this study have been documented thoroughly in a number of previous studies, which include Kang and Thole (2000) and Radomsky and Thole (2000a,b, 2001). A schematic of the stator vane test section and a table showing the relevant geometrical parameters and operating conditions are given in Fig. 1. To allow for highly resolved measurements, the vane was geometrically scaled-up by a factor of nine. The inlet Reynolds number to the test section was matched to that of an engine operating at altitude conditions.

The test section consisted of an instrumented central vane in addition to the leading edges of two adjacent vanes. A flexible plexiglass sidewall, which allowed optical axis for LDV measurements, was attached to the leading edges of the vane. The flexible wall was placed to exactly match the geometry of an adjacent vane. Downstream of where the adjacent airfoil would end, the location of the flexible wall was placed to match the pressure distribution on the central airfoil predicted by a 2-D, low speed, inviscid calculation. Static pressure measurements on the vane were performed to insure the correct placement of the flexible wall in addition to insuring periodic flow was achieved between the two passages.

Heat transfer measurements along the vane mid-span and at the stagnation location were made on the polystyrene central vane, which was wrapped with five, 50 μm thick, type 304, stainless steel foils. The metal foils provided a constant heat flux boundary condition. Beneath the foils and embedded in the styrofoam, 58 type E thermocouples were placed. The spanwise position for the thermocouples was at 40% measured from the bottom endwall. The heat transfer distribution was also measured on the vane endwall with a detailed description of this process given in Kang et al. (1999). The endwall surface started at 4.6 chords upstream of the vane. A boundary layer trip was placed close to the start of the surface to insure a fully turbulent boundary layer at the vane leading edge. The cross-hatched region in Fig. 1 shows the constant heat flux surface used for the endwall heat transfer measurements. The constant heat flux surface consisted of a 50 μm thick copper layer on top of a 75 μm thick kapton layer. Embedded in the kapton layer was a 25 μm thick inconel-heating element arranged in a serpentine pattern. The copper layer was applied on top of the heater to smooth out any temperature gradients that existed between the serpentine patterns of the heating elements. The heat transfer surface was painted black ($\varepsilon = 0.96$) to allow for measurements of the temperatures using an infra-red camera. The camera was calibrated using surface thermocouples, also painted black, placed on the heated endwall surface. For both the mid-span and endwall heat transfer measurements, radiation and conduction corrections were applied to the total input heat flux to give the convective heat flux.

The freestream turbulence was generated using an active grid that had jets being injected in the upstream and downstream directions. The bars were 1.27 cm^2, were placed 1.9 chords upstream of the vane (88 bar widths), and were spaced 17.8 bar widths apart (four bars). The jet holes in the bars were 1.5 mm in diameter and spaced 3.05 cm apart.

Boundary layer measurements were made at nine streamwise locations along the vane using a two component LDV system. The location of boundary layer measurements consisted of four streamwise locations on the pressure surface and five locations along the suction surface (Radomsky and Thole, 2001). In addition, flow field measurements were made surrounding the airfoil (Radomsky and Thole, 2000a) as well as in the endwall-vane juncture region (Kang et al., 1999).

The partial derivative and sequential perturbation methods, described by Moffat (1988), were used to estimate the uncertainties of the measured values. Uncertainties were calculated based on a 95% confidence interval. The estimate of bias and precision uncertainties for the mean velocities were 1% while the precision of the rms velocities was 1.2% for u_{rms} and 1.7% for v_{rms}. The precision uncertainties of the Reynolds shear stress and correlation coefficient were 4.8% and 5.4%. Note that these uncertainty estimates were at the high freestream turbulence conditions near the surface on the suction side of the vane. The total uncertainty in the Stanton numbers was 4% at the leading edge and 5% at the trailing edge on the suction side of the vane. Along the endwall, the uncertainty in Stanton number was 4.5% for the location having the minimum temperature differential. The total uncertainty in the friction factor was a maximum of 7.5% for a laminar boundary layer and 5% for a turbulent boundary layer.

4. Inlet flow conditions

Profiles of the mean velocity and turbulence components were measured at the inlet location as indicated on Fig. 1. Fig. 2(a) shows streamwise and pitchwise mean velocity profiles for both the inner and outer passages. Fig. 2(b) presents the streamwise, pitchwise, and spanwise rms levels also measured at the geometric stagnation location. The high freestream turbulence measurements were compared to a baseline case, measured at low freestream turbulence conditions of $Tu = 0.6\%$, and to a CFD prediction using the Reynolds stress turbulence model (RSM) at freestream turbulence levels of $Tu = 1\%$. The mean velocities have been normalized by the inlet approach velocity, U_{inlet}. A global coordinate system, as shown in Fig. 1 with the origin at the stagnation point of the center vane ($Y/P = 0$), was maintained for the results shown in Fig. 2(a). The measured flowfield clearly indicate periodicity between the inner and outer passages, which is important for insuring good quality flow conditions. Although the turbulence levels were very high, the good agreement with the low freestream turbulence case and CFD prediction shows the mean flowfield was unaffected by the turbulence generator. The anisotropic behavior of the turbulence is indicated by non-uniformity among the velocity rms levels. Although not shown here, the rms levels for all three velocity components at a location one-third chord upstream of the vane showed nearly isotropic turbulence with the average streamwise fluctuations ($u_{\text{rms}}/U_{\text{inlet}}$) being 0.20, the average cross-stream ($v_{\text{rms}}/U_{\text{inlet}}$) being 0.20, and the average spanwise ($w_{\text{rms}}/U_{\text{inlet}}$) being 0.18. The integral and dissipation length scales measured across the passages indicated uniform values. The integral scale was 11% of the pitch while the dissipation scale was 28% of the pitch. For the boundary layer measurements a dense passive grid was used to obtain the same turbulence level and length scale as the active grid (Radomsky and Thole, 2001). An active grid was used for all of the endwall studies.

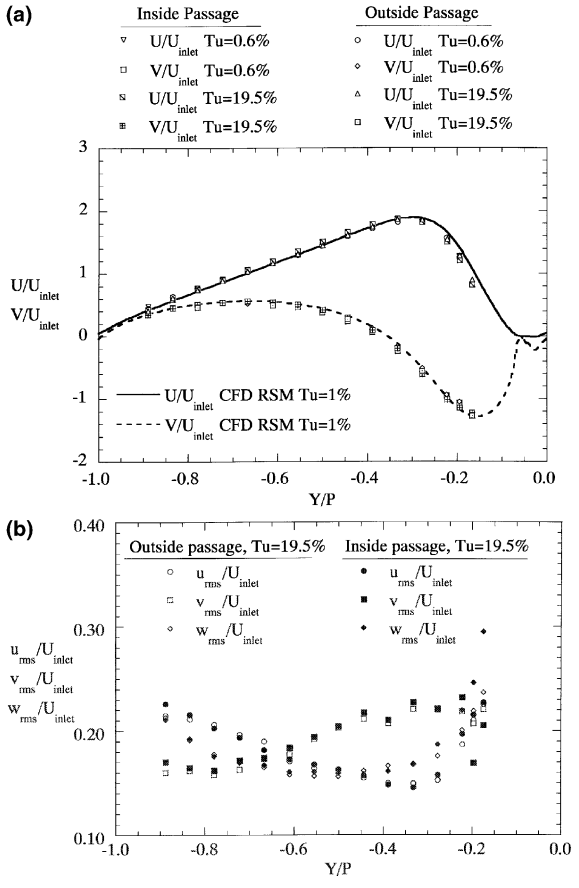

Fig. 2. Measured flow field conditions at the inlet measurement location.

As a check for the boundary layer measurements, a comparison was made between the measured edge velocities, the calculated velocities from the measured static pressure distribution, and the predicted velocities from an inviscid CFD simulation. Fig. 3 shows this comparison and indicates good agreement between the two independent measurements. The positive values of s/C refer to the suction surface, while the negative values indicate the pressure surface. Fig. 3 also illustrates the inviscid velocities affecting the boundary layer development. On the pressure side there is a constant acceleration, with an acceleration factor of $K = 3.4 \times 10^{-6}$ over the majority of the surface, as the flow progresses from the stagnation to the end of the vane. The inviscid velocities along the suction side show a much different behavior with a rapid acceleration up to $s/C = 0.2$ ($1.1 \times 10^{-6} < K < 0.01$). From $s/C = 0.2$ to 0.5, there is a continual acceleration but at a much lower rate ($K = 1.1 \times 10^{-6}$). Beyond $s/C = 0.5$, there is a slight adverse pressure gradient ($K = -1.6 \times 10^{-8}$).

The boundary layer approaching the vane along the endwall surface was maintained similar to that of the low freestream turbulence condition allowing compari-

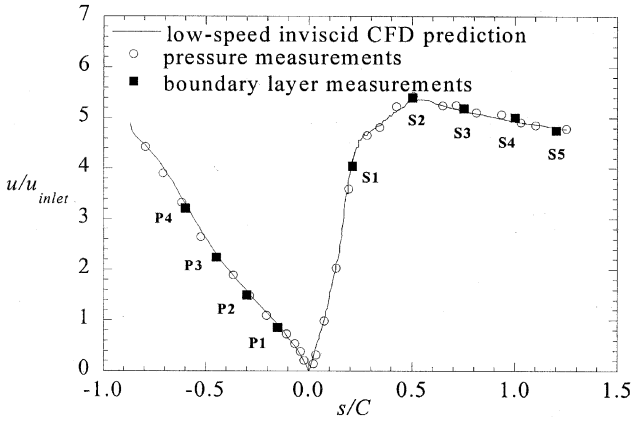

Fig. 3. Comparison of inviscid velocity distribution from static pressure and LDV boundary layer measurements to the low-speed inviscid CFD prediction.

sons of flowfield and endwall heat transfer measurements. The momentum Reynolds number for the low and high turbulence cases were $Re_\theta = 3630$ and 2675 at one-third chord upstream of the vane. Using standard correlations for turbulent boundary layer heat transfer, the 25% difference in Reynolds number should result in a difference in Stanton numbers of 9.5%. As will be shown in the results, the augmentation due to high freestream turbulence was much more than 9.5%. Although the Reynolds numbers were quite similar, the mean velocity profile for the high freestream turbulence condition indicated a much fuller profile with a depressed wake region as compared with the low turbulence.

5. Stagnation point heat transfer

One of the regions exposed to the highest temperatures is the stagnation location of the turbine vane. Figs. 4(a)–(d) provide contours of the velocity fluctuations near the stagnation location of the vane. Note that the normalizing velocity for the fluctuations of each velocity component in the incident velocity (U_{inlet}) while the normalizing velocity for the turbulent kinetic energy is the local total velocity thereby giving the local turbulence level. For the streamwise fluctuations (u_{rms}/U_{inlet}) the inlet levels were uniform across the span at $u_{rms}/U_{inlet} = 0.20$. Near the leading edge, an increase in the streamwise fluctuations occurred with the peak occurring at the flow stagnation location at a value of $u_{rms}/U_{inlet} = 0.24$.

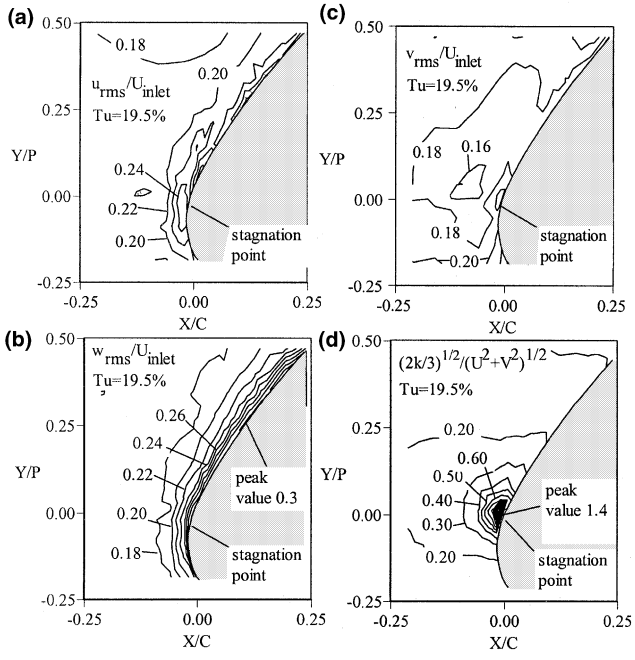

Fig. 4. Velocity fluctuation measurements near the stagnation location of the vane.

The location where the increase in the fluctuations began to occur coincided with one integral length scale upstream of the vane. This increase in the streamwise turbulence level in the stagnation region was the result of the production of turbulence due to the flow deceleration. Closest to the wall at the stagnation location, the streamwise fluctuations decreased as a result of being attenuated by the presence of the vane. The normalized pitchwise rms levels decreased to $v_{rms}/U_{inlet} = 0.16$. The normalized spanwise rms levels (w_{rms}/U_{inlet}), shown in Fig. 4(c), indicate variations only occurred in the near-wall regions. At the inlet, the spanwise rms levels fell just below $w_{rms}/U_{inlet} = 0.20$ with levels that increased to $w_{rms}/U_{inlet} = 0.30$ near the stagnation location. Bearman (1972) showed that although no rate of strain exists in the spanwise direction at the mid-span, large amplifications of the spanwise turbulence can be observed.

Dullenkopf and Mayle (1995) developed a correlation for stagnation heat transfer that contained effects of the freestream turbulence level and freestream strain rates of the flow. Fig. 5 shows a comparison of the current heat transfer results to their correlation at turbulence levels of 0.6%, 10% and 19.5% at and near the vane stagnation location. At the low effective turbulence levels, $Tu_\lambda < 5$, the measurements at each location agree well with the Dullenkopf and Mayle (1995) correlation. At the higher effective turbulence levels, the measurements gradually deviate from the linear correlation. The present experimental results indicate a decreasing sensitivity to turbulence at higher turbulence levels. In addition to the current investigation, Fig. 5 shows results for airfoil heat transfer by Ames (1997) along the stagnation location and pressure surfaces. With the exception of the Schulz (1986) data for heat transfer on the pressure surface of an airfoil, most of the results indicate a deviation from

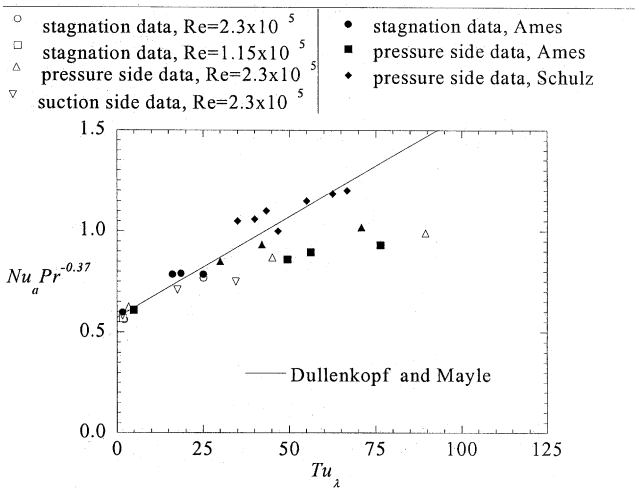

Fig. 5. Turbine vane stagnation heat transfer at high freestream turbulence conditions.

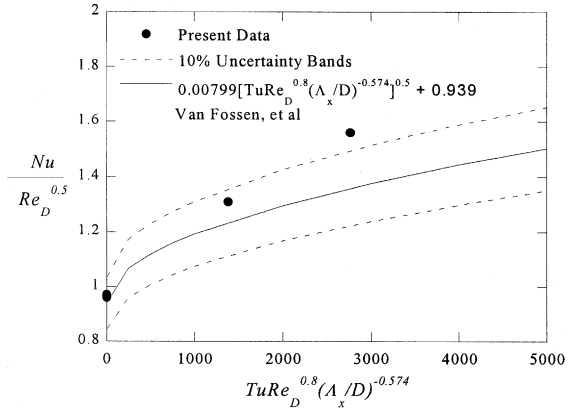

Fig. 6. Turbine vane stagnation heat transfer compared with a Frossling number correlation (Van Fossen et al., 1995).

the correlation at the higher effective turbulence levels ($Tu_\lambda > 30$). Note that the length scales for the Schulz (1986) experiments were not actually measured, but were estimated by Dullenkopf and Mayle (1995) by examining the decay of the turbulence at two streamwise locations.

A correlation presented by Van Fossen et al. (1995) was also compared with the stagnation heat transfer data as shown in Fig. 6. Note that the effective diameter was calculated by performing an inviscid curve fit to the velocity measurements upstream of the stagnation location. While good agreement occurs for the low freestream turbulence case, disagreement between the data and the correlation becomes increasingly larger at the high freestream turbulence levels. This correlation was based on data for circular and elliptical leading edges placed downstream of passive grids. The highest turbulence level that was considered was 15.9% with the largest length scale to diameter ratio of 0.3. The length scale to diameter ratio for our study was 0.3 with the highest turbulence level being 19.5%.

6. Mid-span heat transfer and shear stress

The friction coefficient and the Stanton number distribution at the low turbulence level are plotted for the pressure surface as a function of surface Reynolds numbers in Fig. 7(a). Boundary layer measurements were made at the locations noted on Fig. 3 (P1–P4 and S1–S5) in which the shear stress was determined through a fit to the data in the near wall region. Note that the local edge velocities are used as the velocity scales in Re, C_f, and St and the surface distance from the stagnation location is used in Re. The Stanton number curves for the two inlet Reynolds numbers fall on the same curve for the pressure surface. Both the friction coefficient and heat transfer data indicate the boundary layer remained laminar over the entire surface. The data sets

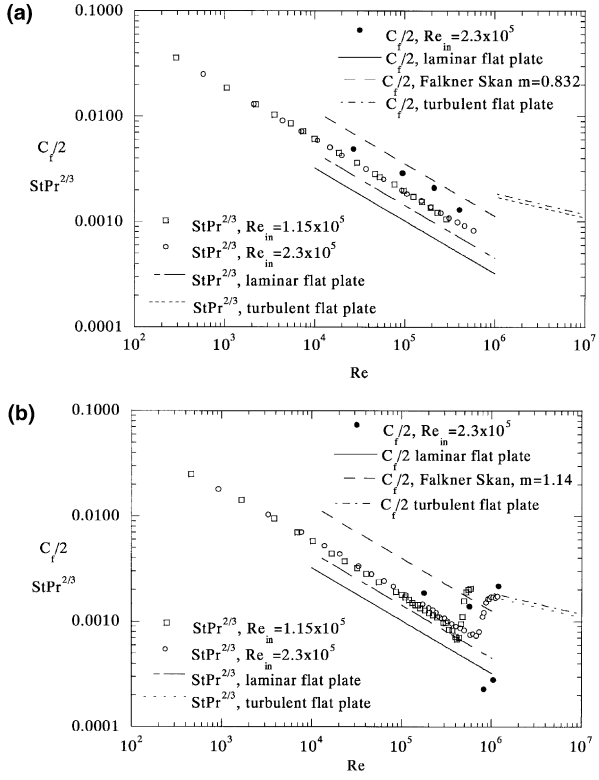

Fig. 7. Comparison of measured Stanton number and friction coefficients on: (a) the pressure surface; (b) the suction surface at $Tu = 0.6\%$.

were above their respective correlations for laminar boundary layer flow over a flat plate. The increased friction and heat transfer is a result of the presence of a favorable pressure gradient caused by the flow accelerating in the vane passage. These data were also compared with a prediction using the Falkner–Skan similarity approach for a laminar boundary layer, which accounts for the streamwise pressure gradients. The friction coefficients fell below the Falkner–Skan prediction, but the agreement was better than observed with the flat plate correlations.

The friction coefficient and the Stanton number distribution at low turbulence level are plotted for the suction surface as a function of surface Reynolds numbers in Fig. 7(b). Both the friction coefficient and heat transfer data initially indicated a laminar boundary layer. As with the pressure surface, the data was above the respective flat plate correlations due to the favorable pressure gradient. The flow was accelerated up to $s/C = 0.5$ ($Re_{\text{in}} = 6 \times 10^5$). The friction coefficient at this location indicates an increase in the slope of the friction coefficient suggesting that transition was beginning at this location. This transition assertion is supported by the velocity measurements, which showed a mean profile that was beginning to appear turbulent and a turbulence profile that showed some fluctuations. Downstream of this location, the boundary layer was subjected to an adverse pressure gradient and the measured friction

coefficient showed a dramatic decrease in magnitude. The decrease in the friction coefficient was the result of the adverse pressure gradient affecting the development of the boundary layer in the near wall region as will be shown later by the boundary layer measurements. Farther downstream, at a location of $s/C = 1.2$ ($Re_{in} = 1.2 \times 10^6$), the measured friction coefficient indicated that transition from a laminar to turbulent boundary layer had been completed.

The Stanton number curve also indicated that transition began near location S2 ($Re_{in} = 5 \times 10^5$) where the friction coefficient initially started to increase. The heat transfer coefficients did not show a dramatic decrease as with the skin friction. Greater effects on the friction coefficients as compared to the Stanton numbers were observed in transitioning boundary layers subjected to adverse pressure gradients in Mislevy and Wang (1996). The Stanton numbers for the two Reynolds numbers initially fell along the same curve in the favorable pressure gradient region. The presence of the adverse pressure gradient caused transition to occur at both Reynolds numbers near the trailing edge.

Fig. 8(a) shows the friction coefficients at 19.5% and Stanton numbers on the pressure surface at 10% and 19.5% turbulence levels. Both the friction coefficient and Stanton numbers indicate that over a majority of the surface a laminar boundary layer was present, with magnitudes higher than those at 0.6% turbulence levels. Fig. 8(b) displays the friction coefficient at 19.5% and Stanton numbers on the suction surface at 10% and 19.5% turbulence levels. Comparisons to Fig. 7(b) show that transition occurs at a lower Reynolds number near $Re_{in} = 4 \times 10^5$ as compared to $Re_{in} = 6 \times 10^5$ at low freestream turbulence conditions. The dip in the friction coefficient is not observed at high freestream turbulence conditions because the boundary layer transitioned prior to the onset of the adverse pressure gradient. This resulted in an increase in momentum in the near wall region which resulted in less of a decrease in the friction coefficient for the adverse pressure gradient under high freestream turbulence.

Fig. 8(c) shows the enhancements of the Stanton number and skin friction due to high freestream turbulence. In general, the heat transfer augmentation was greater than the skin friction augmentation. The heat transfer was augmented by as much as 80% for the highest turbulence levels on the pressure side. The large spikes on the suction side are due to the upstream shift in the transition location.

Figs. 9(a)–(c) shows the mean velocity profiles measured on the pressure surface plotted in terms of inner coordinates at 0.6% and 19.5% turbulence levels and the corresponding turbulent velocity profiles. At low freestream turbulence conditions, shown in Fig. 9(a), all four of the measured profiles on the pressure surface indicated an expected laminar boundary layer. At the

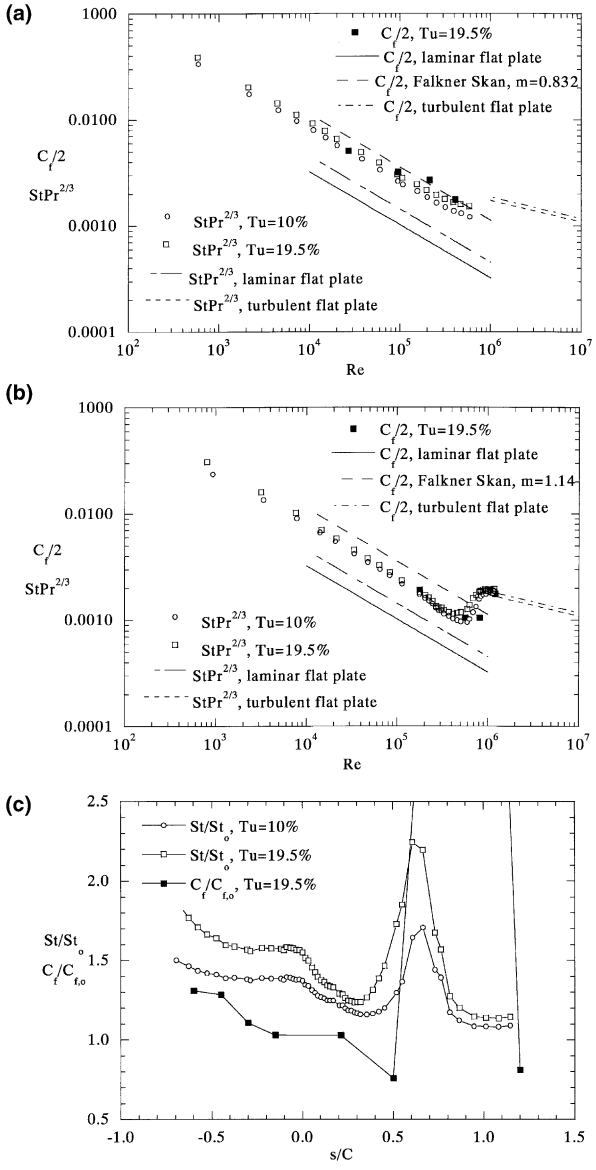

Fig. 8. Comparison of measured Stanton number and friction coefficients on: (a) the pressure surface; (b) the suction surface at $Tu = 19.5\%$; (c) augmentations due to turbulence.

high freestream turbulence conditions, the boundary layer profiles exhibited the same behavior and, as expected from the increased shear stress, lower u^+ values at the boundary layer edge.

The streamwise (u_{rms}) and normal (v_{rms}) fluctuations are plotted showing maximum levels near a $y^+ = 20$. For a turbulent boundary layer, the maximum value of the streamwise rms levels were 2.8 and occur at a location near $y^+ = 15$. For the first three streamwise positions (P1, P2 and P3) the maximum level in the boundary layer reached levels of 2.2 at a location of $y^+ \sim 20$. At location P4, the streamwise rms levels are higher reaching levels similar to those in a turbulent boundary layer. Moving closer to the wall, a sharp

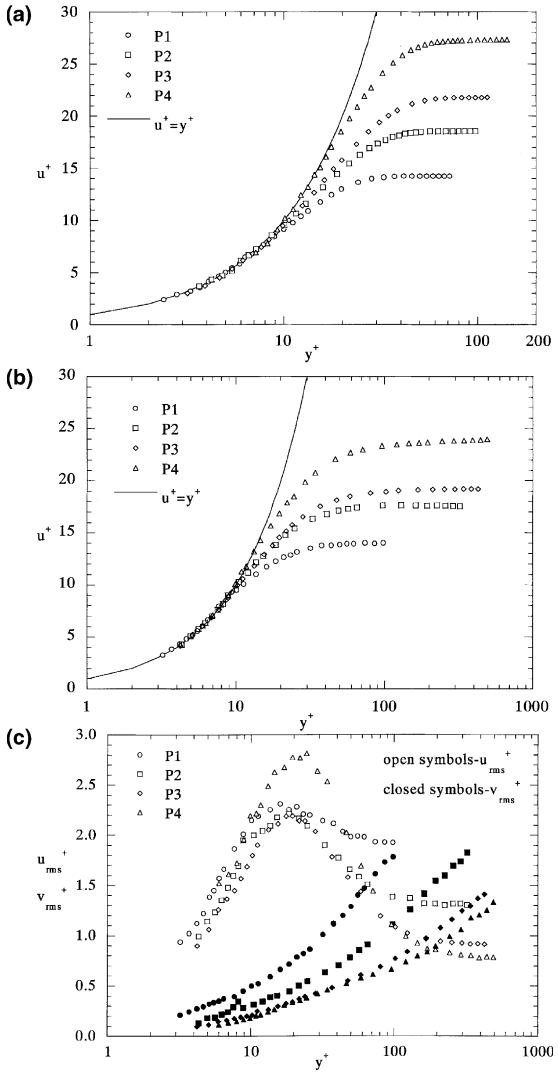

Fig. 9. Boundary layer profiles on the pressure surface at: (a) $Tu = 0.6\%$; (b) $Tu = 19.5\%$. Turbulence levels are shown in (c) for $Tu = 19.5\%$.

decrease in the streamwise rms levels was observed. Recall that the acceleration parameter was $K = 3.4 \times 10^{-6}$ along the pressure side of the airfoil. With such a large acceleration, one would expect that any boundary layer transition would be suppressed by the acceleration. The previously shown mean velocity profiles and calculated shape factors are in agreement with typical laminar profiles, but the large fluctuations indicate the presence of turbulence. The normal rms (v_{rms}) levels show a continual decrease in magnitude as the stator vane surface is approached as a result of being attenuated by the vane surface. It is interesting to note that the location of the peak fluctuating value is further away from the wall than that which would occur for a turbulent boundary layer profile along a flat plate. Fig. 9(c) also indicates the anisotropy of the freestream turbulence outside the boundary layer, which is a result of the redistribution of the turbulence due to streamline curvature and acceleration.

A number of correlations are available in the literature that scale the augmentation of heat transfer due to high freestream turbulence effects. Those correlations were derived for turbulent boundary layers in which the freestream turbulence level was elevated. One intent of those studies, however, has been to capture the augmentations relative to what would occur along an airfoil. A few of these correlations have been applied to the data taken for this study and are shown in Figs. 10(a)–(c). All of these correlations underpredict the augmentation. Albeit, all of these correlations were developed for flat plate turbulent boundary layers and, as seen from the velocity profiles, this does not typically occur over the majority of the turbine vane.

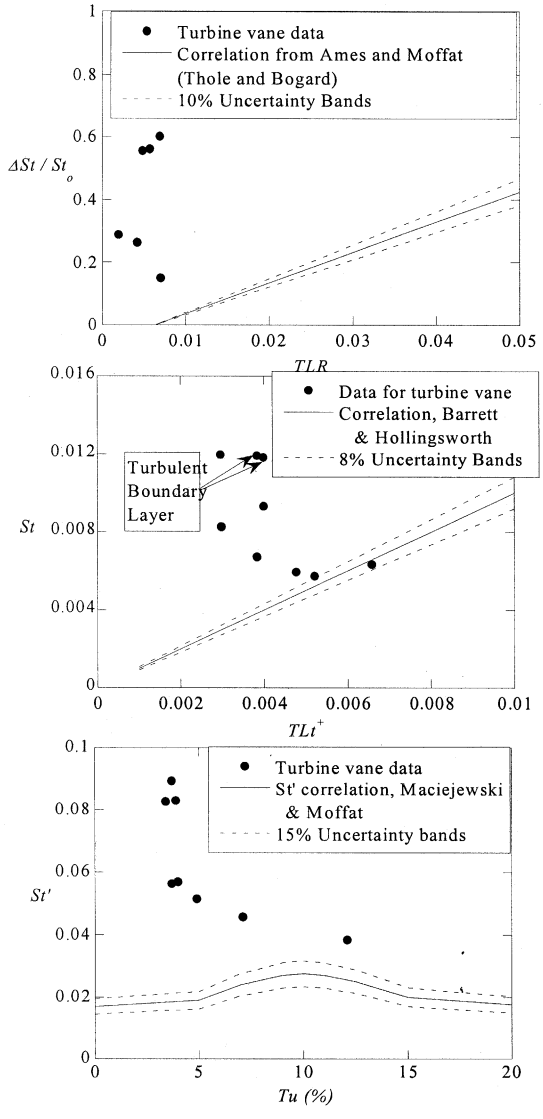

Fig. 10. Mean and turbulent velocity measurements in the vane-endwall juncture for $Tu = 0.6\%$ and 19.5%.

7. Endwall heat transfer

There are no correlations available to quantify the effect that high freestream turbulence has on heat transfer in the endwall (platform) region of a turbine airfoil. Accounting for the heat transfer in this region, however, is crucial for having a durable airfoil design. The reason it is difficult to predict the heat transfer in this region of the airfoil is because of the secondary flow pattern that develops through the passage. The secondary flows are comprised of a leading edge horseshoe vortex (Figs. 11(a)–(d)), which splits about the stagnation location, and a passage vortex that develops as the flow is turned by the vane.

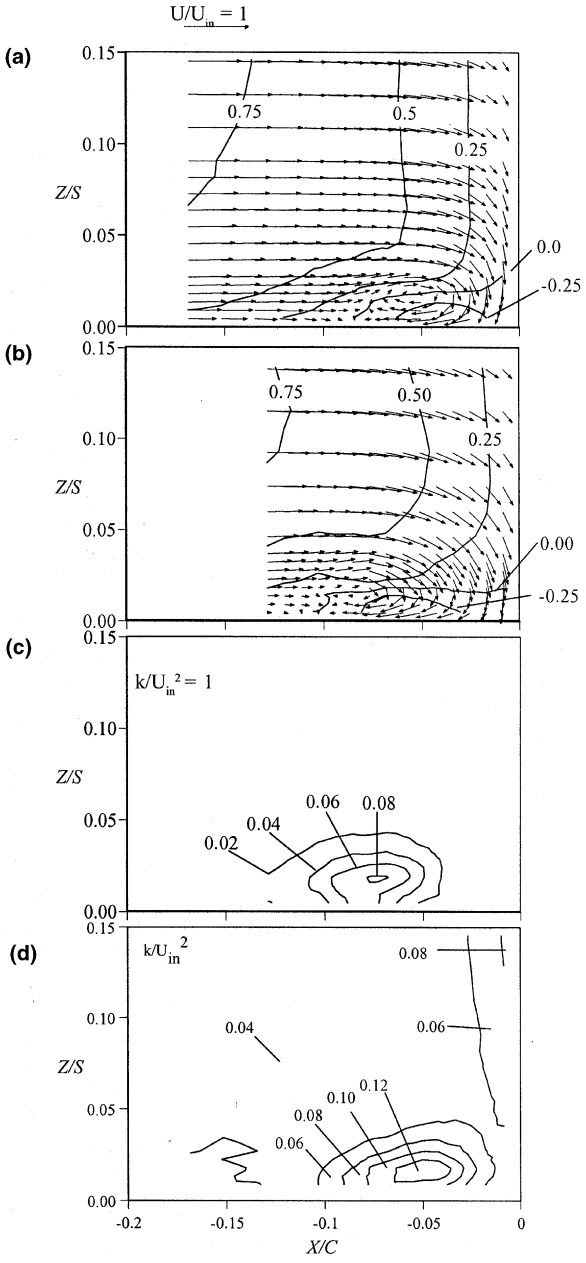

Fig. 11. Mean and turbulent velocity measurements in the vane-endwall juncture for $Tu = 0.6\%$ (a), (c) and 19.5% (b), (d).

A comparison of the leading edge horseshoe vortices and fluctuating velocities for low and high freestream turbulence cases are shown in Figs. 11(a)–(d). Recall this measurement plane is parallel with the incoming flow direction and intersects the vane surface at the stagnation location. Superimposed on the velocity vectors (U and W) are contours of the streamwise (U/U_∞) velocity. The primary difference between the low and high freestream turbulence cases is that for the high freestream turbulence case the vortex is located slightly closer to the vane surface and there is more of a complete roll-up than for the low freestream turbulence case. The height of the vortex core for the two cases are very similar with the location being in the near-wall region at approximately $Z/S = 0.015$. Having the vortex pushed closer to the vane for the high turbulence case can be explained by the fact that near the wall the fluid velocity is faster for the high freestream turbulence case, due to the fuller boundary layer profile, as compared with the low freestream turbulence case. This is an effect of the high freestream turbulence flattening out the approaching boundary layer profile.

The turbulent kinetic energy contours shown in Figs. 11(c) and (d) for the low and high freestream turbulence conditions indicate that the primary difference is higher turbulent kinetic energy levels occurring for the high turbulence case. Compared with the low freestream turbulence case, the peak turbulent kinetic energy levels are located closer to the vane surface. This is consistent with the vortex center being closer to the vane surface. If one compares the level of streamwise fluctuation with those found in a canonical turbulent boundary layer, it is evident that the fluctuations are much higher in the vortex region. These high levels are in agreement with the data previously presented by Devenport and Simpson (1990) who associated these high fluctuations with an unsteady motion of the horseshoe vortex.

The heat transfer results plotted in terms of a Stanton number based on the inlet velocity are given in Fig. 12(a) for the high freestream turbulence case. Although it is not shown here for the low freestream turbulence case, the heat transfer contour pattern is similar between the low and high freestream turbulence cases. A region of high heat transfer is observed in front of the vane stagnation point as a result of the formation of the horseshoe vortex. The strong downward flow, previously shown in the flowfield measurements, causes high heat transfer levels swept near the suction surface. Farther into the vane passage, the Stanton number contours become aligned parallel to the direction of flow. High Stanton number contours are observed near the flexible wall as a result of the passage vortex impinging on the endwall surface. Lower Stanton number values are observed near the suction surface of the stator

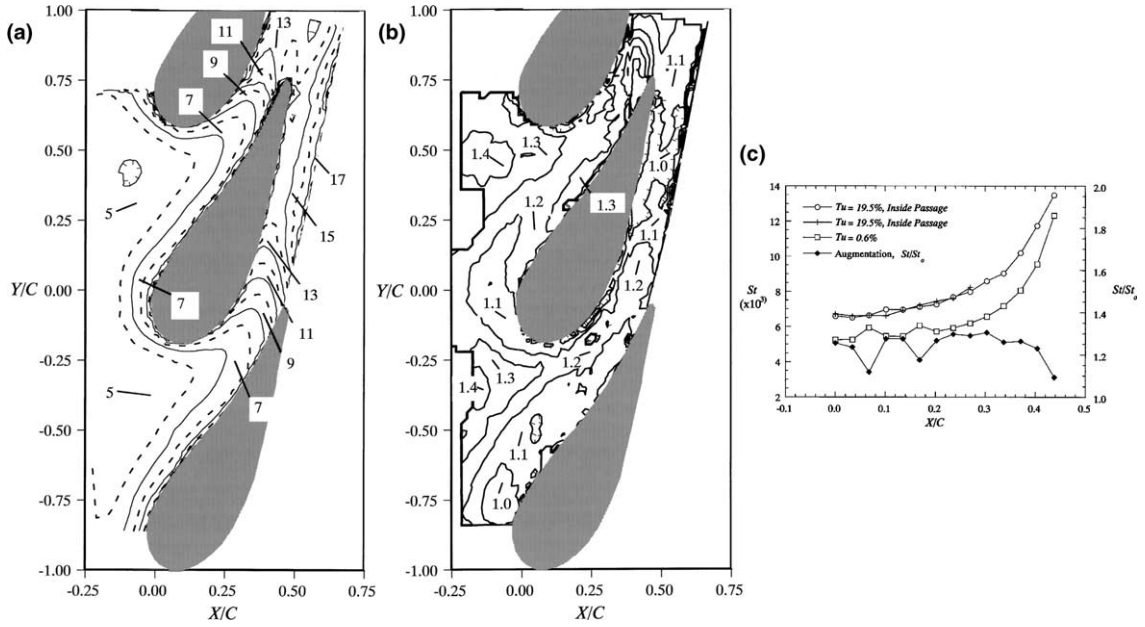

Fig. 12. Heat transfer measurements along the vane endwall for (a) $Tu = 19.5\%$ as compared with the augmentations (b), (c).

vane where the passage vortex is lifting the flow away from the endwall. As a result of the higher turbulence levels, higher values for the Stanton number are observed throughout the vane endwall. Near the trailing edge of the stator vane, however, the Stanton number levels are very similar, with only slightly higher values being seen for the higher turbulence level. This would suggest that in this region, the heat transfer is being dominated by the secondary flow effects rather than high freestream turbulence effects. In addition, the high velocities at this location result in lower overall turbulence levels.

Fig. 12(b) indicates the augmentation of the heat transfer due to high freestream turbulence. The augmentation is defined as the Stanton number occurring at high freestream turbulence (St) conditions divided by the Stanton number at low freestream turbulence (St_0) conditions. The augmentation was calculated by defining a small region, averaging the Stanton number in that area for both the low and high turbulence cases at a given location, and then dividing the two quantities. The defined region was that of a circle with a radius equal to the averaging area of the infra-red camera. Superimposed on the contours shown in Fig. 11(b) is the trajectory of the center of the passage and leading edge vortices based on the flowfield measurements reported by Kang and Thole (2000) for the low freestream turbulence case. Given the fact that the leading edge horseshoe vortex mean flowfield was close to the same for both the low and high freestream turbulence cases, it is reasonable to presume that the path of the passage vortex is much the same for the two cases. Fig. 12(b) indicates the lowest augmentation levels occur in the regions with the most intense vortex action. These low contour levels can be tracked coming off the leading edge as the leading edge horseshoe vortex develops into a passage vortex. The passage vortex then sweeps from the pressure side to the suction side, which also coincides with much lower augmentation levels. These results indicate that the heat transfer in the region of the vortices (leading edge and passage) is dictated by the vortices rather than the elevated turbulence level augmentation. Fig. 12(c) compares the heat transfer coefficients averaged across the pitch for a range of axial position. In addition, Fig. 12(c) illustrates good agreement between data taken in both passages surrounding the central airfoil for the high freestream turbulence case. For most of the axial distance, the augmentation is relatively constant at 25% above the low freestream turbulence case. Only near the end of the vane where the passage vortex dominates, beyond X/C of 0.38, is there a decrease in the augmentation.

8. Conclusions

Detailed heat transfer measurements on a turbine vane geometry at combustor representative turbulence levels have been compared to measurements at low turbulence levels. For this study the following three regions of the airfoil have been emphasized: the stagnation location, the mid-span, and the endwall.

The results indicated that the correlations developed from simple cylinders-in-cross-flow and flat plate studies are not adequate in predicting augmentations in heat transfer for a turbine vane at combustor level turbulence

levels. For the stagnation location, the velocity fluctuations were shown to be quite anisotropic and increasing in magnitude in the approach to the vane. Along the mid-span, the augmentation in heat transfer along the pressure side was as high as 80% above the low freestream turbulence case. The mean velocity measurements indicated a laminar-like mean profile even though fluctuations were present. Since many of the correlations were derived for a turbulent boundary layer under low and high freestream turbulence conditions, it is not surprising that these correlations do not correctly predict the augmentation. For the endwall region, the augmentation was nominally 25% about the low freestream turbulence case with the lowest augmentation occurring in the region of the strongest secondary flows.

Acknowledgements

The authors would like to acknowledge the Department of Energy-Advanced Gas Turbine Systems Research Program and Pratt and Whitney for their support.

References

Ames, F.E., Moffat, R.J., 1990. Heat transfer with high intensity, large scale turbulence: the flat plate turbulent boundary layer and the cylindrical stagnation point. Stanford University, Report No. HMT-44.

Ames, F.E., 1997. The influence of large-scale high-intensity turbulence on vane heat transfer. ASME J. Turbomachinery 119, 23–30.

Barrett, M.J., Hollingsworth, D.K., 1999. On the correlation of heat transfer in turbulent boundary layers subjected to freestream turbulence, National Heat Transfer Conference, NHTC99-76.

Barringer, M., Richard, O., Walter, J., Stitzel, S., Thole, K.A., 2001. Flow field simulations of a gas turbine combustor. ASME Paper 2001-GT-0170.

Bearman, P.W., 1972. Some measurements of the distortion of turbulence approaching a two-dimensional bluff body. J. Fluid Mech. 53, 451–467.

Devenport, W.J., Simpson, R.L., 1990. Time-dependent and time-averaged turbulence structure near the nose of a wing-body junction. J. Fluid Mech. 210, 23–55.

Dullenkopf, K., Mayle, R.E., 1995. An account of free-stream turbulence length scale on laminar heat transfer. ASME J. Turbomachinery 117, 401–406.

Goebel, S.G., Abuaf, N., Lovett, J.A., Lee, C.P., 1993. Measurements of combustor velocity turbulence profiles, 93-GT-228.

Hancock, P.E., Bradshaw, P., 1983. The effect of freestream turbulence on turbulent boundary layers. ASME J. Fluids Eng. 105, 298–306.

Kang, M., Kohli, A., Thole, K.A., 1999. Heat transfer flowfield measurements in the leading edge region of a stator vane endwall. ASME J. Turbomachinery 121, 558–568.

Kang, M., Thole, K.A., 2000. Flowfield measurements in the endwall region of a stator vane. ASME J. Turbomachinery 122, 458–466.

Kestin, J., 1966. The effect of freestream turbulence on heat transfer rates. In: Advances in Heat Transfer, 3. Academic Press, New York.

Kuotmos, P., McGuirk, J.J., 1989. Isothermal flow in a gas turbine combustor – a benchmark experimental study. Exp. Fluids 7, 344–354.

Maciejewski, P.K., Moffat, R.J., 1992. Heat transfer with very high freestream turbulence: part II – analysis of results. ASME J. Heat Transfer 114, 827–833.

Mislevy, S.P., Wang, T., 1996. The effects of adverse pressure gradients on momentum thermal structures in transitional boundary layers: part 1 – mean quantities. ASME J. Turbomachinery 118, 717–727.

Moffat, R.J., 1988. Describing the uncertainties in experimental results. Exp. Thermal Fluid Sci. 1, 3–17.

Radomsky, R., Thole, K.A., 2000a. Highly turbulent flowfield measurements around a stator vane. ASME J. Turbomachinery 122, 255–262.

Radomsky, R., Thole, K.A, 2000b. High freestream turbulence effects in the endwall leading edge region. ASME J. Turbomachinery 122, 699–708.

Radomsky, R., Thole, K.A., 2001. Detailed boundary layer measurements on a turbine stator vane at elevated freestream turbulence levels, 2001-GT-0169.

Schulz, A., 1986. Zum Einfluss hoher Freistromturbulenz intensiver Kuehlung und einer Nachlaufstroemung auf den aeusseren Waermeruebergang einer konvektiv gekuelten Gasturbinenschaufel, Ph.D. dissertation, University of Karlsruhe.

Thole, K.A., Bogard, D.G., 1995. Enhanced heat transfer and shear stress due to high freestream turbulence. ASME J. Turbomachinery 117, 418–424.

Van Fossen, G.J., Simoneau, R.J., Ching, C.Y., 1995. Influence of turbulence parameters, Reynolds number body shape on stagnation-region heat transfer. ASME J. Heat Transfer 117, 597–603.